inorganics

MDPI

Article

A Novel Fluorescent Chemosensor Based on Rhodamine Schiff Base: Synthesis, Photophysical, Computational and Bioimaging Application in Live Cells

Oyedoyin Aduroja, Roosevelt Shaw, Sisay Uota, Isaac Abiye, James Wachira and Fasil Abebe *

Department of Chemistry, Morgan State University, 1700 E Cold Spring Ln, Baltimore, MD, 21251 USA; oyolo1@morgan.edu (O.A.); roosevelt.shaw@morgan.edu (R.S.); siuot1@morgan.edu (S.U.); isaac.abiye@morgan.edu (I.A.); james.wachira@morgan.edu (J.W.)

* Correspondence: fasil.abebe@morgan.edu

Abstract: A novel rhodamine-6G derivative **RdN** was synthesized by condensing rhodamine glyoxal and 3-hydroxy-2-naphthoic hydrazide using a microwave irradiation-assisted reaction. Colorimetric and photophysical studies have demonstrated that the molecule produced can selectively sense Pb^{2+} and Cu^{2+} ions in a solution of CH_3CN/H_2O (9:1, v/v). The spirolactam ring of **RdN** opens upon complexation with the cations, forming a highly fluorescent complex and a visible color change in the solution. The compound **RdN** was further studied with the help of computational methods such as the Density Functional Theory (DFT) method and time-dependent density theory (TD-DFT) calculations to study the binding interactions and properties of the molecule. DFT calculations and job plot data supported the 2:1 complex formation between **RdN** and Pb^{2+}/Cu^{2+}. The limit of detection for Pb^{2+} was determined to be 0.112 μM and 0.130 μM for Cu^{2+}. The probe **RdN** was applied to the image of Pb^{2+} and Cu^{2+} ions in living cells and is safe for biomedical applications. It is used to monitor Pb^{2+} in environmental water samples.

Keywords: microwave-assisted synthesis; rhodamine 6G; colorimetric; fluorescence; probe; computational; bioimaging

Academic Editor(s): Name

Received: date
Revised: date
Accepted: date
Published: date

Citation: Aduroja, O.; Shaw, R.; Uota, S.; Abiye, I.; Wachira, J.; Abebe, F. A Novel Fluorescent Chemosensor Based on Rhodamine Schiff Base: Synthesis, Photophysical Properties, Computational and Bioimaging Application in Live Cells. *Inorganics* **2025**, *12*, x. https://doi.org/10.3390/xxxxx

1. Introduction

Due to the importance and toxicity of heavy metal to living organisms, there is a great demand for developing sensors for sensing and quantifying heavy metal ions in biological and environmental samples [1]. Lead is considered a hazardous metal ion; even deficient concentrations of Pb^{2+} exposure is irreversible and can cause a long-lasting danger to human health [2–5]. The U.S. Environmental Protection Agency sets the maximum contamination level for lead in drinking water at 15 μgL^{-1} [6]. Conversely, copper is an essential element in humans and is available at low levels in various tissues and cells, with higher amounts in the liver [7]. Excess copper ions in the cytoplasm can cause Alzheimer's [7] and Parkinson's disease [8]. Therefore, simple and cost-effective lead and copper ions detection methods in environmental and biological samples are essential. Fluorescent sensing is preferable to other methods because of its sensitivity and simplicity [8]. Several probes for Pb^{2+} [1–5] and Cu^{2+} [7–10] ions were investigated; however, problems and challenges exist. Most limitations include target ions' selectivity, sensitivity, water solubility, and tedious synthetic procedures.

The rhodamine framework is ideal for building fluorescent probes due to its fluorescence on/off mechanism, which controls the interconversion between the non-fluorescent spirolactam and the ring-opened fluorescent tautomer. This structural change has been widely applicable for many years and used as a recognition mode to construct colorimetric and fluorescent probes [14–19]. Fluorescence turn-on probes for Pb^{2+} based on rhodamine derivatives in living cells are still a very active and significant challenge now and in the future. Many investigators are still searching for simple, more stable, convenient, and effective rhodamine derivatives.

Considering these, this paper synthesized a 3-hydroxy-2-naphthoic hydrazide-modified rhodamine 6G derivative, **RdN**. It is a highly Pb^{2+} and Cu^{2+} selective and sensitive colorimetric and fluorescent probe in aqueous solution and living cells. The synthesis route of the proposed compound **RdN** is shown in Scheme 1.

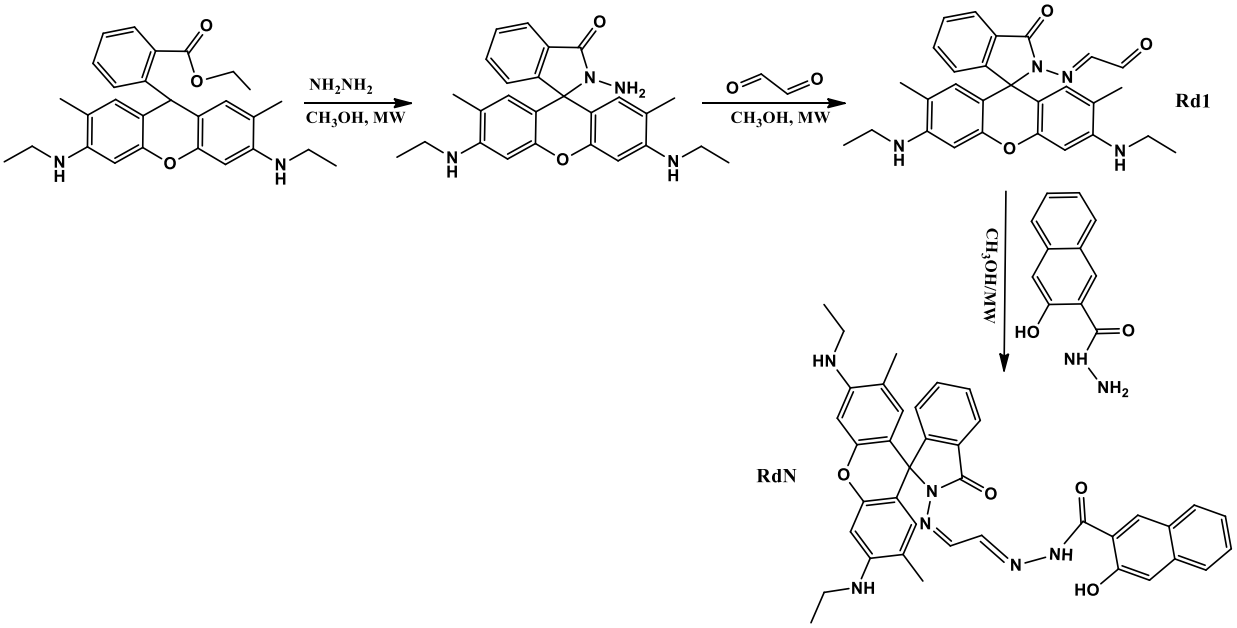

Scheme 1. Microwave irradiation-assisted synthesis of **RdN**.

2. Results and Discussion

2.1. Photophysical Studies

The detection ability of **RdN** was investigated by UV/Vis's absorption and fluorescence spectroscopy. The optical properties of **RdN** towards different cations were examined in the absence and presence of various metal ions such as Na^{+}, K^{+}, Mg^{2+}, Ca^{2+}, Fe^{3+}, Ni^{2+}, Cu^{2+}, Cd^{2+}, Pb^{2+}, Al^{3+}, Cr^{3+}, and Zn^{2+} in CH_3CN/H_2O solution (9/1 v/v, Tris-HCl buffer, pH = 7.2). The metal ion detection studies showed that **RdN** is very sensitive and selective towards Pb^{2+} and interference from Cu^{2+}. As shown in Figure 1a, the rhodamine-based sensor demonstrates a characteristic peak of the spirolactum ring-opened amide form at 530 nm with a shoulder at 490 nm. The new absorption band increases gradually and is saturated at two equivalents of Pb^{2+} ions, as shown in Figure 1b. However, probe **RdN** exhibited distinguishable naked-eye sensing properties toward Pb^{2+} and Cu^{2+}. The optical photographs under 350 UV light indicated a noticeable fluorescence emission change, as shown in Figure 2.

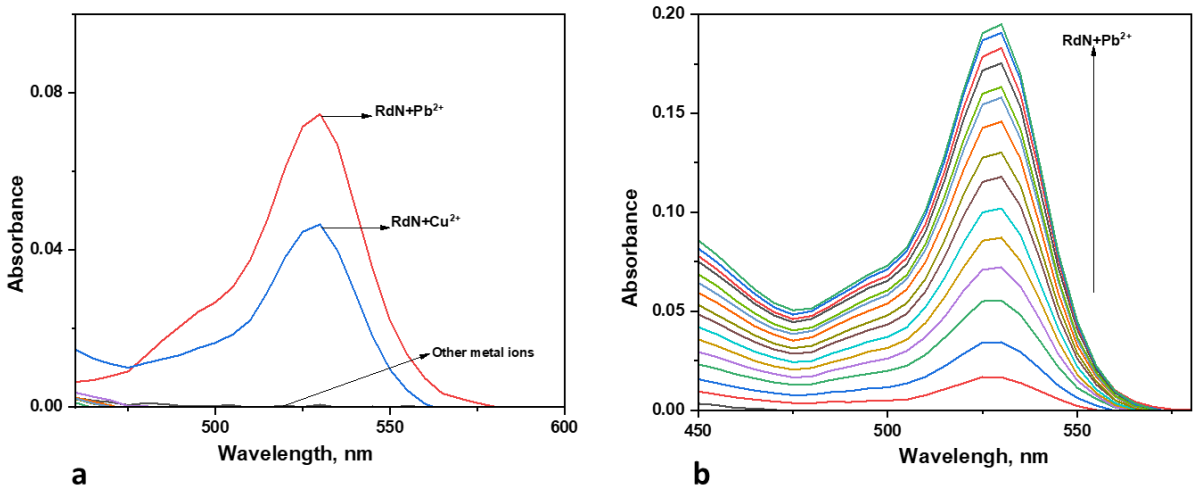

Figure 1. (**a**) UV-Vis absorption spectra of **RdN** (10μM) with various cations. (**b**) UV-Vis absorption titration of **RdN** (10μM) with Pb^{2+} (0–20μM) in acetonitrile-water (9:1 v/v) buffer solution.

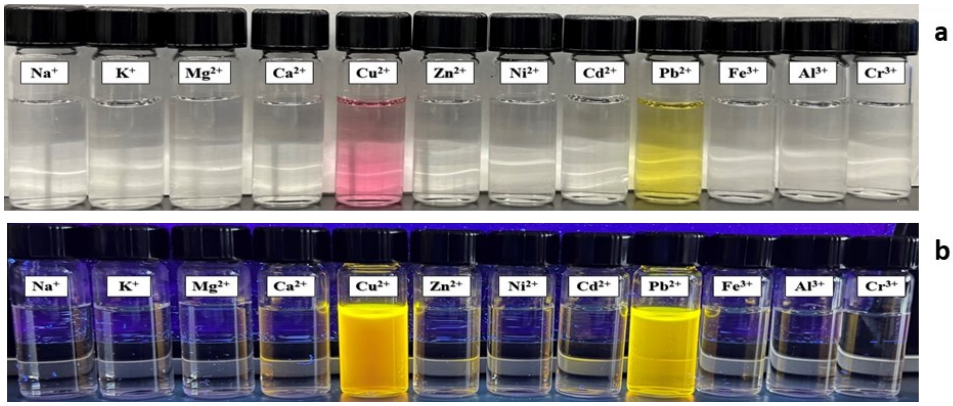

Figure 2. The visual color of sensor **RdN** (**a**) and the fluorescence under UV illumination after adding various metal ions (**b**).

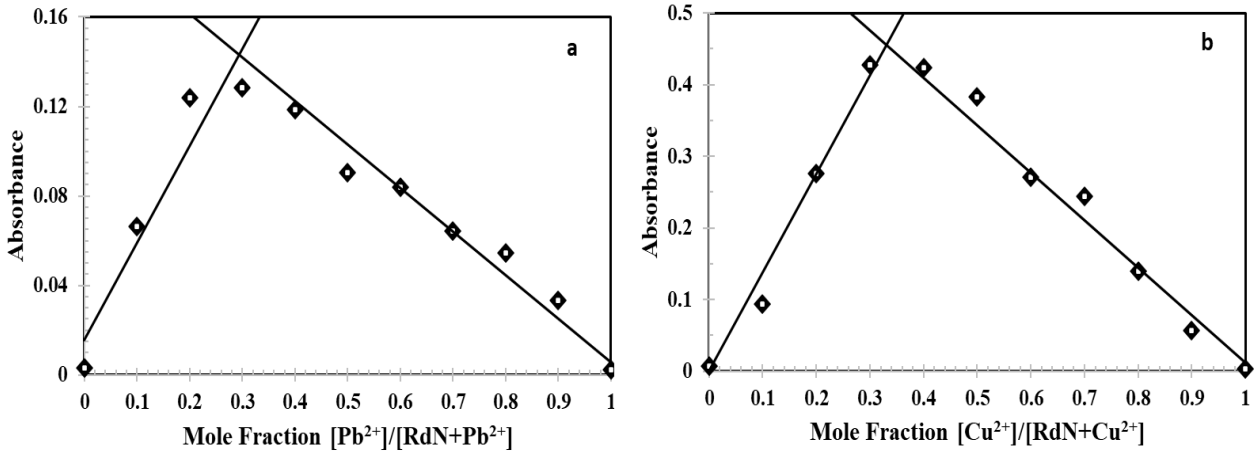

Figure 3. (**a**) Job's plot analysis of **RdN** versus Pb^{2+} at a total concentration of 10μM. (**b**) Job's plot analysis of **RdN** versus Cu^{2+} at a total concentration of 10μM.

The fluorescence changes of **RdN** were investigated in the same CH_3CN/H_2O solution upon adding various metal ions. As shown in Figure 4a, the sensor **RdN** alone is non-

fluorescent when excited at 490 nm. The study revealed that the interaction of Pb^{2+} and Cu^{2+} induced a significant fluorescent enhancement at 560 nm. The change in fluorescence intensity is attributed to the ring-opened spirolactam amide form of **RdN** that binds with the ions. The fluorescence titration of **RdN** was carried out with the subsequent addition of Pb²+, and a steady increase in emission intensity was observed at 560 nm, as illustrated in Figure 4b. The unique selectivity of **RdN** to Pb2⁺ may be due to the combination of the size effect and the Hard-Soft principle [15]. Based on the 3δ/S (δ: standard deviation; S: slope) formula, the detection limits of **RdN** for Pb^{2+} and Cu^{2+} were determined to be 0.112 μM and 0.130 μM, respectively, from the titration plot of the absorbance. The standard deviation was determined by measuring the blank solution 10 times (n = 10). These results signified that **RdN** could operate as a "turn-on" type fluorescent sensor for both metal ions. The results are compared with reported literature in Table 1. The effect of pH on the fluorescence of **RdN** was investigated in a pH range of 3 to 11. For free **RdN** at pH < 5, as shown in Figure 5a, the open ring of spirolactum became protonated, which caused an evident change in color and an increase in fluorescence intensity. Therefore, all measurements were performed in a buffer solution with a pH of 7 to maintain the sensor in ring-closed form. The addition of various anions (CH_3COO^-, N_3^-, HSO_4^-, CN^-, S^{-2}, ClO_3^-, NO_2^-, CO_3^{2-}, F^-, Cl^-, and Br) to the **RdN**-Pb^{2+} (1:1) solution, of which cyanide (CN^-) alone quenches the fluorescence intensity. The results strongly support the idea that **RdN**-Pb^{2+} binds CN^- ions with high selectivity, and the process demonstrates reversibility of the sensor, as shown in Figure 5b. The proposed binding mechanism of the sensor with Pb^{2+} with and without CN^- is shown in Scheme 2.

The fluorescence lifetime of the sensor **RdN** with Pb^{2+} was examined to confirm the sensor's photophysical properties. The binding of Pb^{2+} in the sensor **RdN** had a significant impact on the lifetime of the rhodamine derivative. The experiment showed second exponential characteristics in the free **RdN** and **RdN**-Pb^{2+} complexes. As shown in Figure S1, the **RdN**-Pb^{2+} complex had the highest longevity compared to the free rhodamine derivative **RdN.** Lead (II) ions influence a rhodamine-based molecule's time in the ground and excited states before emitting a photon.

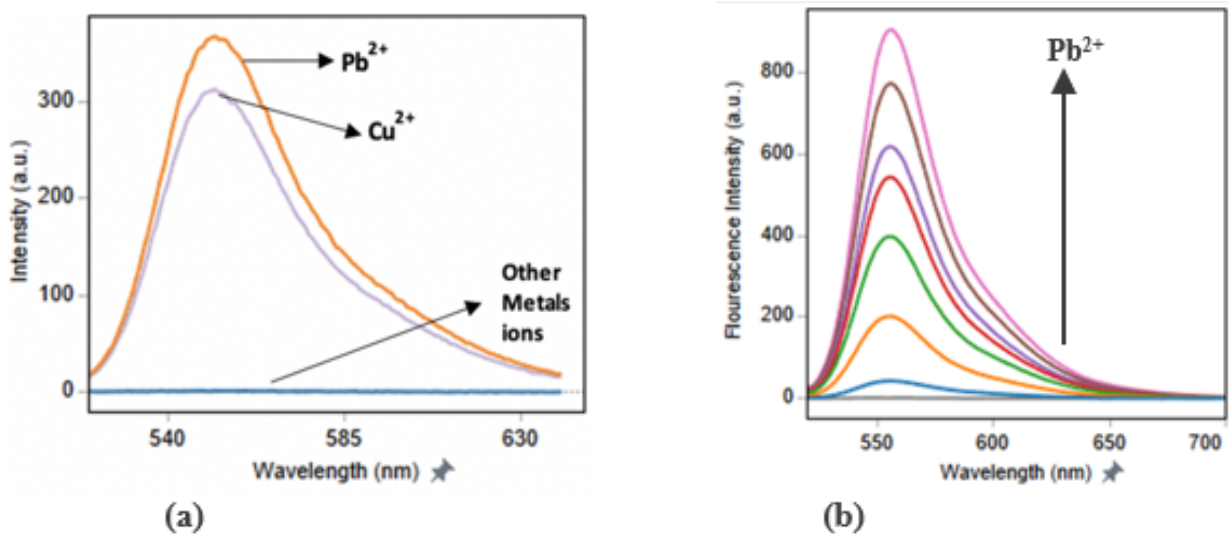

Figure 4. (**a**) Fluorescence spectra of **RdN** (5μM) with cations (λ_{exc}: 490 nm). (**b**) Fluorescence emission titration of **RdN** with Pb^{2+} (0–15μM) acetonitrile-water (9:1 v/v) solution.

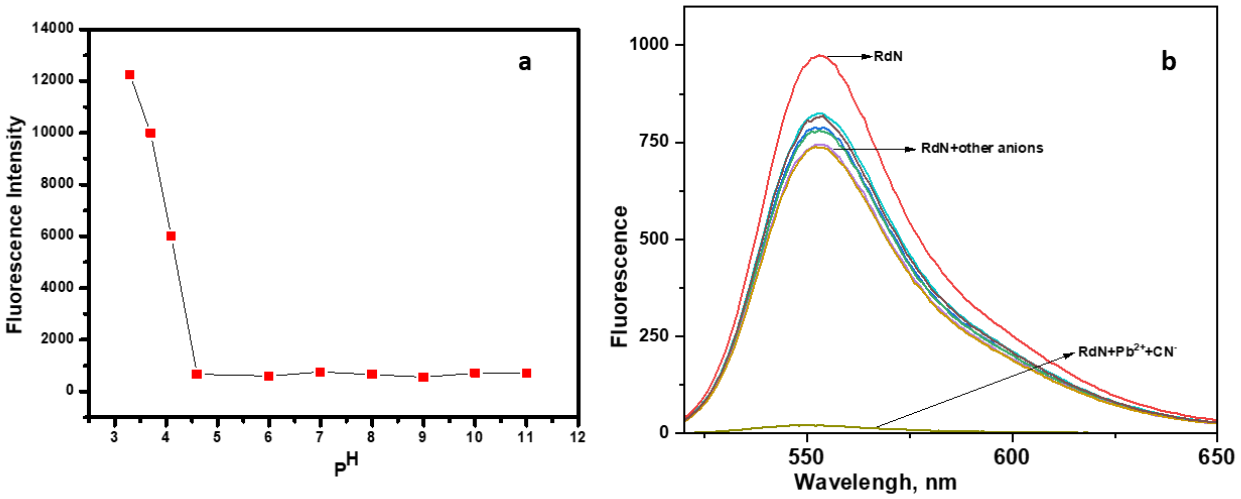

Figure 5. (**a**) Effect of pH on fluorescence intensity of sensor **RdN** (10μM) (**b**) Fluorescence spectra of **RdN**-Pb^{2+} complex (1:1) in the presence of various anions (Cl^{-}, Br^{-}, F^{-}, CH_3COO^{-}, HSO_4^{-}, CN^{-}, ClO_3^{-}, NO_2^{-}, S^{-2}, N_3^{-}, CO_3^{2-}).

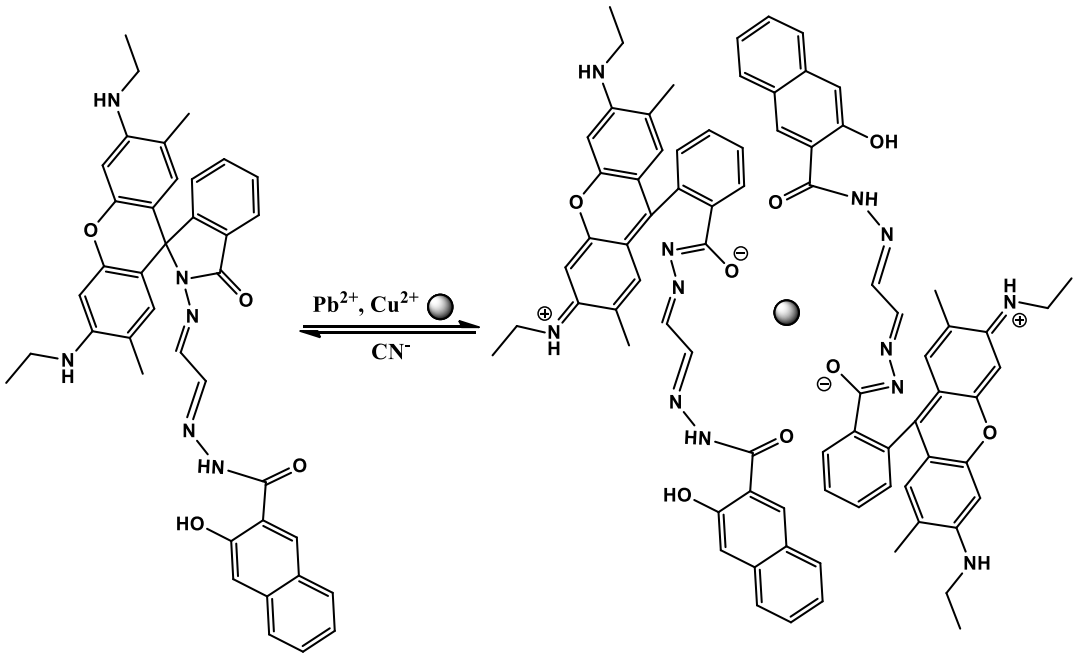

Scheme 2. The 1:2 binding stoichiometry of lead/copper ions and reversibility of CN^{-} on **RdN**-cation complex.

Table 1. Analytical performance of the probe **RdN** compared to other previously published Pb^{2+} probes. (HEPES:4-(2-hydroxyethyl)-1-piperazineethanesulfonic acid)

Sensor	Media	Reversible	LOD (μM)	Detected cation	Refs.
Rhodamine B	CH_3Cl: THF	Yes	-	Pb^{2+}	[16]
Rhodamine B	EtOH:HEPES	No	0.86	Pb^{2+}/Al^{3+}	[17]
Rhodamine 6G	HEPES	No	0.0027	Pb^{2+}	[18]
Rhodamine 6G	C_2H_5OH: H_2O	Yes	0.016	$Pb^{2+}/Hg^{2+}/Cd^{2+}$	[19]
Imidazoquinazoline	CH_3CN: H_2O	Yes	0.69	$Pb^{2+}Fe^{3+}$	[20]
Coumarin	CH_3CN: HEPES	No	0.50	Pb^{2+}	[21]

Anthracene	MeOH: H_2O	Yes	0.94	Pb^{2+}	[22]
Rhodamine B	H_2O:C_2H_5OH	Yes	0.01	Pb^{2+}	[23]
Xanthone	DMSO: H_2O	No	0.18	Pb^{2+}	[24]
Rhodamine B	2% DMSO	Yes	0.112	Pb^{2+}	[25]
Fluorescein	HEPES	Yes	0.017	Cu^{2+}	[26]
Fluorescein	CH_3CN/H_2O	Yes	0.64	Cu^{2+}	[27]
Fluorescein	C_3H_6O	No	0.024	Cu^{2+}	[28]
Rhodamine B	C_2H_5OH: Tris	No	2.94	Cu^{2+}/Cd^{2+}	[29]
Rhodamine B	CH_3CN: H_2O	Yes	2.11	Cu^{2+}	[30]
Rhodamine 6G	CH_3CN: H_2O	Yes		Pb^{2+}/Cu^{2+}	This work

2.2. Sensing Mechanism

The sensor **RdN** solution transitioned from colorless to yellow and pink interaction with Pb^{2+} and Cu^{2+}. This phenomenon is due to the characteristic spirocyclic opening of the rhodamine 6G derivative, which results in the coordination of Pb^{2+} and Cu^{2+} ions. We conducted an analysis using a jobs plot through absorbance measurements to ascertain the binding mode between sensor **RdN** and Pb^{2+}, as well as Cu^{2+}. The highest absorbance at 530 nm was recorded when the mole fraction of Pb^{2+} and Cu^{2+} was close to 0.3, as shown in Figures 3a and 3b. The results suggest that Pb^{2+} and Cu^{2+} bind to **RdN** in a 1:2 stoichiometry. FTIR analysis further confirmed the sensor's complex formation with Pb^{2+} and Cu^{2+}. In a sensor, the imine bond, -C=N-, stretching frequency, and C=O starching frequency appeared at 1640 cm^{-1} and 1725 cm^{-1}, respectively. After interacting with Pb^{2+} and Cu^{2+}ions to the receptor **RdN**, these peaks diminished due to the metal ions' direct binding to the carbonyl oxygen of the rhodamine group and imine bond nitrogen, as shown in Figure 6. The theoretical studies of the sensor and metal ion binding also confirm the coordination of Pb^{2+} and Cu^{2+} to the receptor.

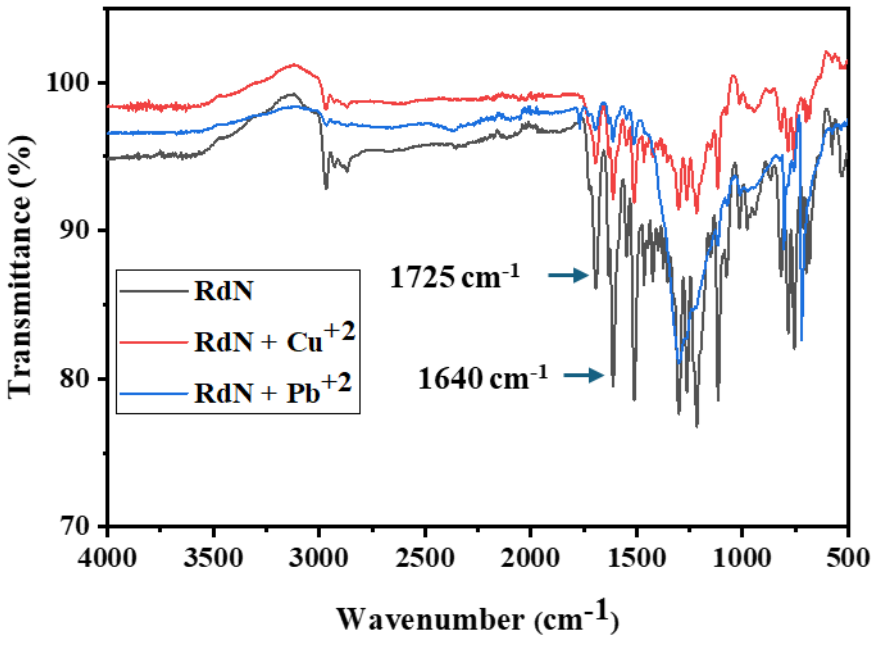

Figure 6. FTIR spectra of free **RdN** and in the presence of Pb^{2+} and Cu^{2+} ions.

2.3. Environmental Analysis

Environmental samples, such as lake, river, pond, and municipal tap water, were used to assess the applicability of **RdN** for determining Pb^{2+}. River and tap water were collected from the Morgan State University campus, and pond and lake water were collected from Hillcrest Park Pond and Lake Roland. The samples were filtered and spiked with a standard solution of Pb^{2+} at concentrations of 3 μM and 6 μM to be analyzed by UV/Vis's spectroscopy. The quantified concentrations for the tap water were 2.991 μM and 5.985 μM; river water 2.986 μM and 6.021 μM; lake water 3.021 μM and 5.986 μM; and pond water samples 2.987 μM and 5.988 μM. The percentage of spiked Pb^{2+} recovered from the water sample ranged from 99.5% to 100.7%, with a relative standard deviation (RSD) of less than 1.00%, as indicated in Table 2. These remarkable recoveries and RSD demonstrate the successful detection of the spiked Pb^{2+} ions by the sensor **RdN**. The results confirm the sensor **RdN'**s capability in determining Pb^{2+} in environmental water samples.

Table 2. Lead (Pb^{2+}) determination in environmental water samples.

Water sample	Spiked (μM)	Found ($\bar{x}^a$ ±SD[b]) (μM)	Recovery (%)	RSD* (%), n = 3
Tap water	3.0	2.991 ± 0.006	99.7	0.20
	6.0	5.985 ± 0.009	99.8	0.15
River water	3.0	2.986 ± 0.008	99.5	0.27
	6.0	6.021 ± 0.008	100.4	0.13
Lake water	3.0	3.021 ± 0.004	100.7	0.13
	6.0	5.986 ± 0.009	99.8	0.15
Pond water	3.0	2.987 ± 0.075	99.6	2.51
	6.0	5.988 ± 0.078	99.8	1.30

[a] Mean of three individual measurements. [b] SD: standard deviation. * RSD: relative standard deviation.

2.4. Time-Dependent Density Functional Theory (TD-DFT) Investigation

To understand better the coordination geometry of the interaction of the sensor with Pb^{+2}, forming **bis-(RdN)$_2$Pb^{+2}** complex, and said sensor with Cu^{+2}, forming bis-**(RdN)$_2$Cu^{+2}** complex, Density-Functional Theory (DFT) method and time-dependent density functional theory (TD-DFT) calculations were performed on these species in the gas phase and both simulated water and acetonitrile media using a conductor-like polarizable continuum model (CPCM). Spartan '20 and '24 software packages provided Cartesian coordinates to obtain Gaussian 09W and Gauss View 06 optimized structures for the above species. For both Spartan and Gaussian calculations, the same level of theory, B3LYP functional and basis set LanL2DZ, was employed. Vertical electronic absorptions and emission data obtained from this investigation provided excellent theoretical insight and support for the empirical results of the interactions of both Pb^{+2} and Cu^{+2} with sensor **RdN**.

Sensor **RdN** can exist as two distinct equilibrium conformers, **RdN I** and **RdN II** (Scheme 3). Frequency calculations and free energy determination of both were carried out in all three media above to determine which equilibrium conformer is of minimum energy. Conformer **RdN II** was found to be the more stable of the two in all three media, owing to the presence of a stabilizing intramolecular hydrogen bond between the amide oxygen and the ortho-hydroxy hydrogen in the 3-hydroxy-2-naphthoic acid moiety. In **RdN I**, these two groups with anti-orientation are too far apart to interact and thus cannot form a stabilizing intramolecular hydrogen bond. Calculated Gaussian Standard Energies of Formation (E) for the two conformers revealed **RdN II,** in the gas phase, to be more stable than **RdN I** by 27.09 kJ/mol; in simulated water, **RdN II** by 6.11 kJ/mol; and in simulated acetonitrile **RdN II** by 4.01 kJ/mol, corresponding to equilibrium concentrations for **RdN II of** 100%, 92% and 84%, in these three media, respectfully.

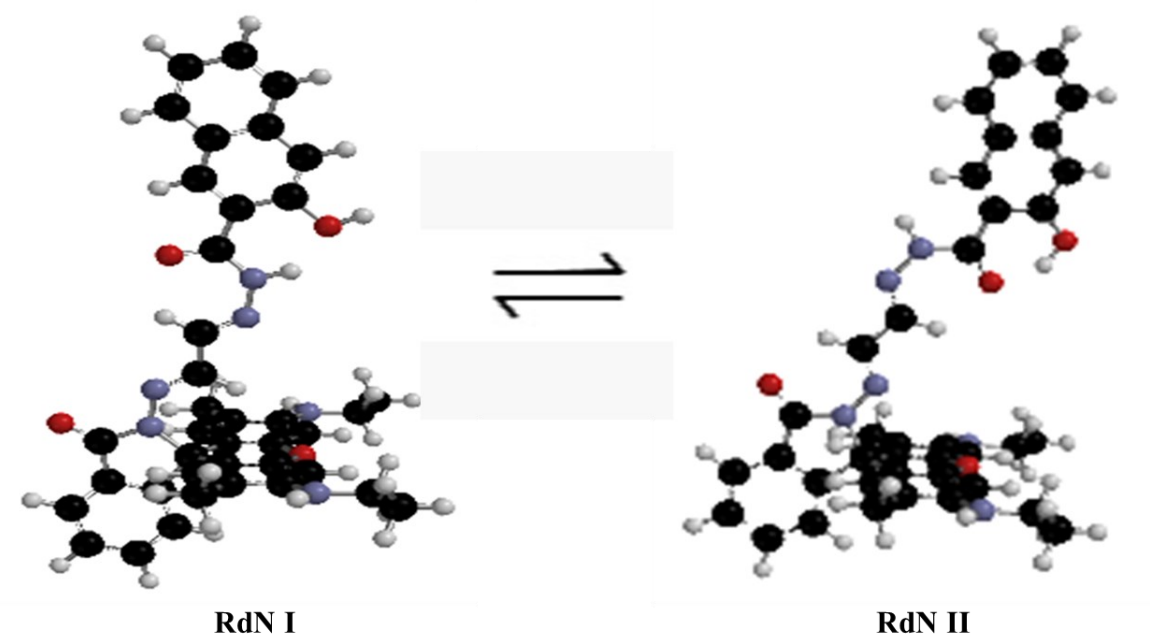

Scheme 3. Optimized Equilibrium conformers **RdN I** and **RdN II** of Sensor **RdN** in the gas state and simulated water and acetonitrile.

In the gas phase, the frontier molecular orbital energy gap (ΔE) for **RdN II** is 2.93 eV (HOMO = −5.32 eV and LUMO = −2.39 eV). HOMO of **RdN II** is found along the ethereal anthracene moiety of rhodamine glyoxal, while LUMO includes the 3-hydroxy-2-naphthoic acid amide, two conjugated imino groups, and the aromatic spirolactam ring moieties. Upon formation of **bis- (RdN II)$_2$Pb^{+2}** complex from **2RdN II** and **Pb^{+2}** in this same medium, the frontier molecular orbital energy gap decreased from 2.93 eV for **RdN II** to 2.11 eV for said complex (HOMO = −9.05 eV and LUMO = −6.94 eV). The HOMO of said complex is located over one of the two xanthene moieties, including most of both attached diethyl amino groups. LUMO is centered about Pb^{+2} in the five-membered heterocyclic ring, which extends to one of the naphthoic acid hydrazide moieties, as shown in Figure 7.

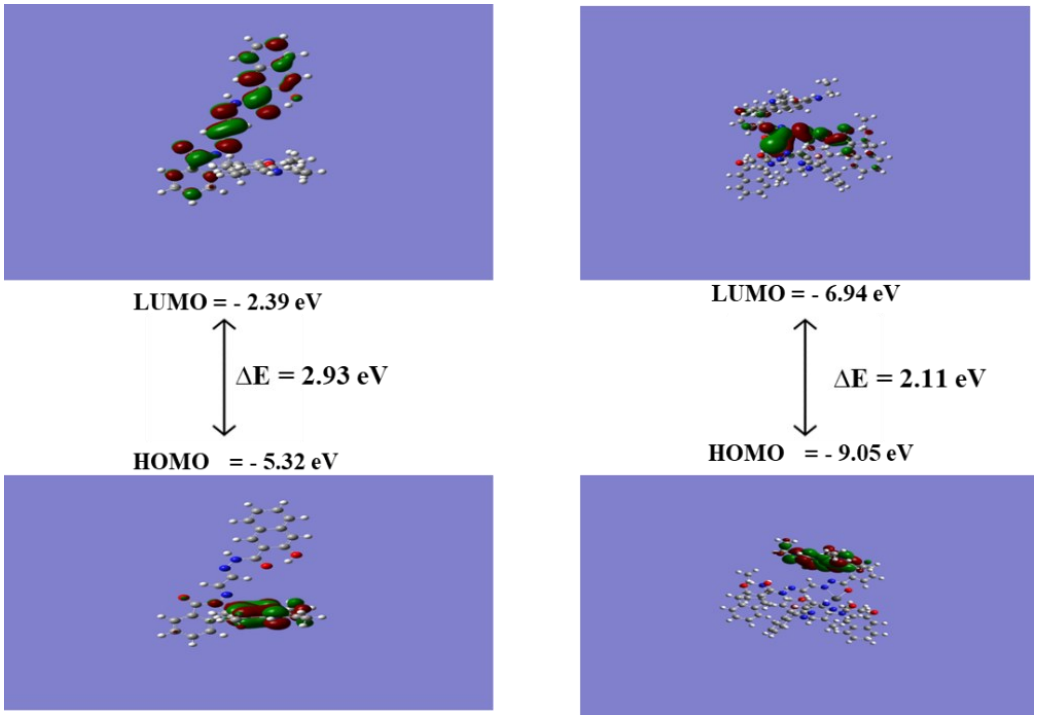

Figure 7. Optimized Structures and Frontier Molecular Orbitals of **RdN II** and **bis-(RdN II)$_2$ Pb^{+2}** complex in Gas State.

In simulated water, the energy gap (ΔE) for **RdN II** is 2.71 eV (HOMO = −5.39 eV and LUMO = −2.68 eV), and both the locations of HOMO and LUMO are unchanged from those observed in vacuum. The corresponding LUMO-HOMO energy gap (ΔE) for **bis-(RdN II)$_2$Pb^{+2}** complex in simulated water is 2.35 eV, a decrease of 0.36 eV in energy from the sensor to complex (HOMO = −5.91 eV and LUMO = −3.56 eV). Both HOMO and LUMO of **bis-(RdN II)$_2$ Pb^{+2}** complex in simulated water mirror those in the gas phase. In simulated acetonitrile, the frontier energy gap (ΔE) for **RdN II** is 2.72 eV (HOMO = −5.39 eV and LUMO = −2.67 eV), roughly the same frontier energy gap as in simulated water (ΔE = 2.71 eV). Both HOMO and LUMO of **RdN II** in simulated acetonitrile mirror the energy distribution of their counterparts in simulated water. Upon formation of **bis-(RdN II)$_2$Pb^{+2}** complex from **2 RdN II and** Pb^{+2} in CH_3CN, the energy gap (ΔE) decreased by 0.36 eV, from 2.72 eV for sensor to 2.36 eV for complex (HOMO = 5.97 eV and LUMO = 3.62 eV). Also, both HOMO and LUMO of **bis-(RdN II)$_2$** Pb^{+2} complex in simulated CH_3CN mirror those observed in both the gas phase and simulated water, as shown in Figure 8.

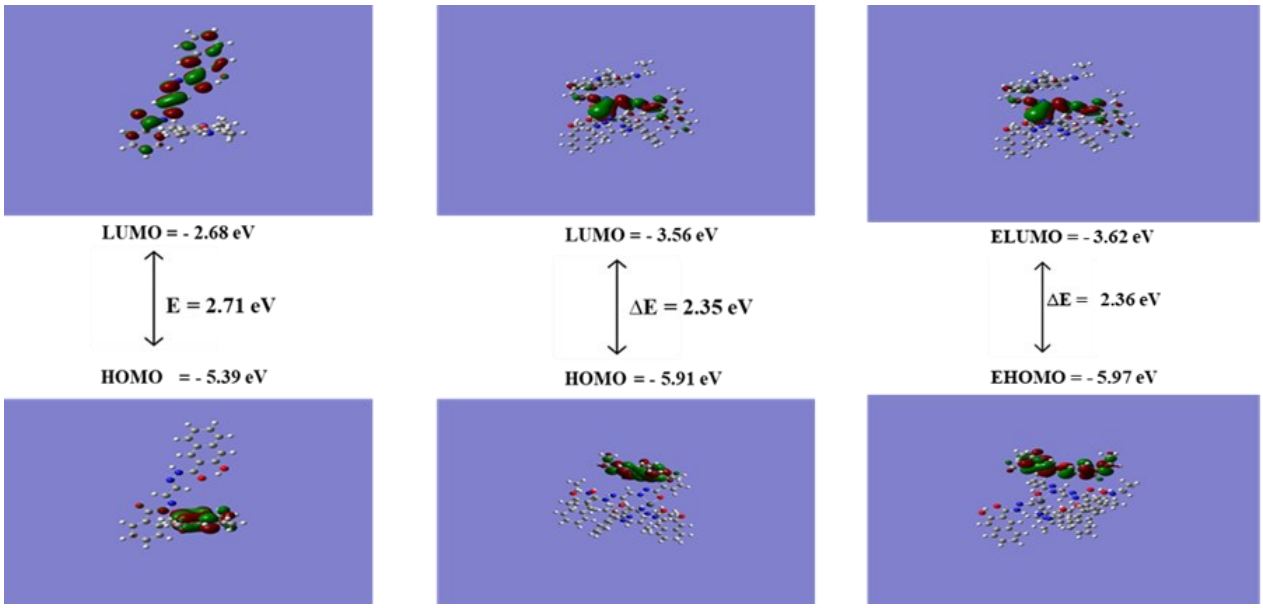

Figure 8. Optimized Structures and Frontier Molecular Orbitals of **RdN II**, **bis-(RdN II)$_2$Pb^{+2}** complex in simulated water medium, and **bis-(RdN II)$_2$ Pb^{+2}** complex in simulated CH_3CN medium.

On formation of **bis-(RdN II)$_2$Cu^{+2}** complex from **2RdN II** and Cu^{+2} in the gas phase, the frontier energy gap (ΔE) decreased from −2.93 eV for said sensor (HOMO = −5.32 eV and LUMO = −6.32 eV) to −2.39 eV for said complex (HOMO = −8.71 eV and LUMO = −6.32 eV). HOMO of **bis-(RdN II)$_2$Cu^{+2}** is located exclusively about the naphthalene ring of one of the two 3-hydroxy-2-naphthoic acid hydrazide moieties. LUMO is found along one of the rhodamine's glyoxal moieties and does not include the attached ethyl groups of the two amino groups, as shown in Figure 9. On formation of **bis-(RdN II)$_2$Cu^{+2}** complex from **2RdN II** and **Cu^{+2}** in the simulated water, the frontier energy gap (ΔE) decreased from 2.71 eV for said sensor (HOMO = −2.68 eV and LUMO = −5.39 eV as presented earlier) to 2.64 eV for **bis-(RdN II)$_2$Cu^{+2}** complex (HOMO = −5.88 eV and LUMO = −3.24 eV). HOMO of **bis-(RdN II)$_2$Cu^{+2}** is found exclusively along one of the two rhodamine glyoxal moieties. Still, it does not include the ring oxygen, while LUMO includes the spirocyclic rings and extends outward into the two hydrazide moieties but does not include Cu^{+2}. In simulated acetonitrile, the energy gap dropped from 2.72 eV for said sensor to 2.69 eV for complex

(HOMO = −5.90 eV and LUMO = −3.21 eV); Both HOMO and LUMO of **bis-(RdN II)$_2$ Cu^{+2}** complex observed in simulated CH_3CN mirror the exact positions of the frontier molecular orbitals found in simulated water, as shown in Figure 10.

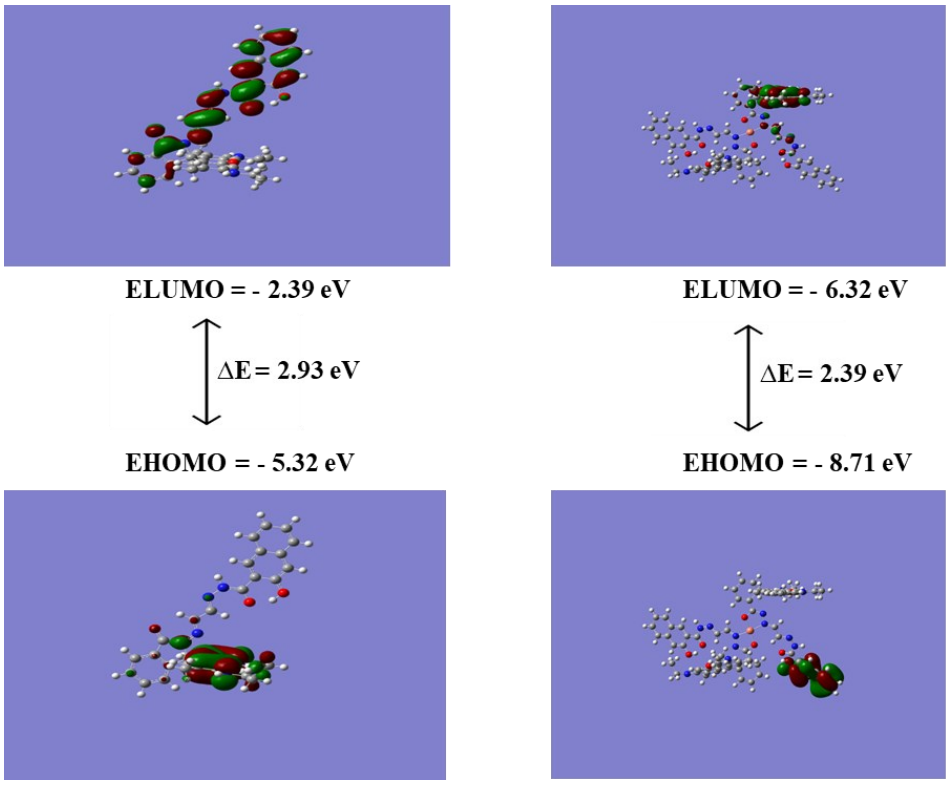

Figure 9. Optimized Structures and Frontier Molecular Orbitals of **bis-(RdN)$_2$Cu^{+2}** in the Gas State.

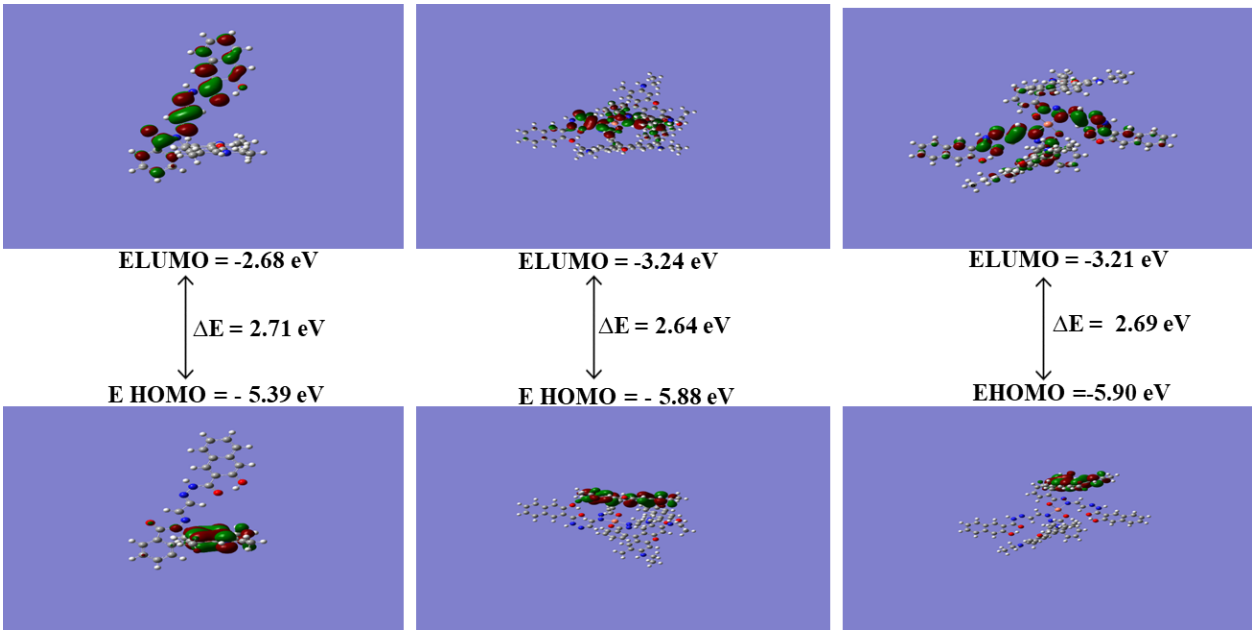

Figure 10. Optimized Structures and Frontier Molecular Orbitals of **RdN II**, **bis-(RdN II)$_2$ Cu^{+2}** complex in simulated water medium, and **RdN II**, **bis-(RdN II)$_2$ Cu^{+2}** complex in simulated CH_3CN medium.

2.5. Cytotoxicity Assay

The cytotoxicity of sensor **RdN** in living cells was evaluated using Methyl Thiazolyl Tetrazolium (MTT) assay [31]. CAD cells were seeded in triplicate in 96-well culture

clusters with a density of 100 μL per well at 5.0 × 10^4 cells/mL and incubated under the required conditions. A concentration gradient ranging from 125 to 4000 μg/L was used to prepare **RdN** (10 mM in DMSO) solutions, which were then washed with phosphate-buffered saline. The cells were incubated for 4 h with 5.0 mg/mL MTT solution. Subsequently, 100 μL of detergent solution was introduced into each well to dissolve the crystals formed, followed by measuring the absorbance at 570 nm. The cytotoxicity of **RdN** in CAD cells after 24 h was measured and presented in Figure 11. In the experiment, the toxicity of **RdN** in CAD cells was shown to be less than 15% at a dosage of 1000 μg/L. This concentration is significantly greater than the threshold of μmol/L $Pb^{2+,}$ which is considered harmful in biological systems [31]. Therefore, the results indicate that incubating CAD cells with **RdN** for 24 h has a minimal harmful impact.

2.6. Cellular Imaging

The fluorescence imaging analysis is conducted in CAD cells to examine the potential use of compound **RdN** in biological samples. After the cells were seeded on eight well-covered glass chamber slides (ibid USA, Inc. Fitchburg, Wisconsin), they were allowed to adhere overnight before being imaged. The CAD cells were washed with buffer solution and then incubated with **RdN**-containing medium at a concentration of 10 μM for 30 min at 37o C. Then, they were supplemented with Pb2+ at a concentration of 10 μM for an additional 30 min. After being washed with PBS buffer, the intracellular region emits a significant fluorescence, as illustrated in Figure 12, and Figure 13 shows the same phenomenon for Cu^{2+}. These results indicate that the probe **RdN** penetrates the cell membrane and can be used for in vivo imaging of Pb^{2+} and Cu^{2+} in living cells.

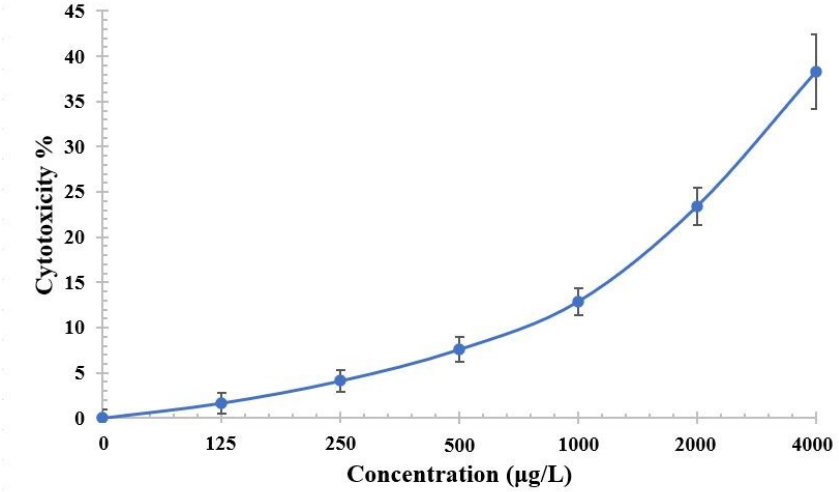

Figure 11. The compound **RdN** cytotoxicity study on CAD cells in 24 h.

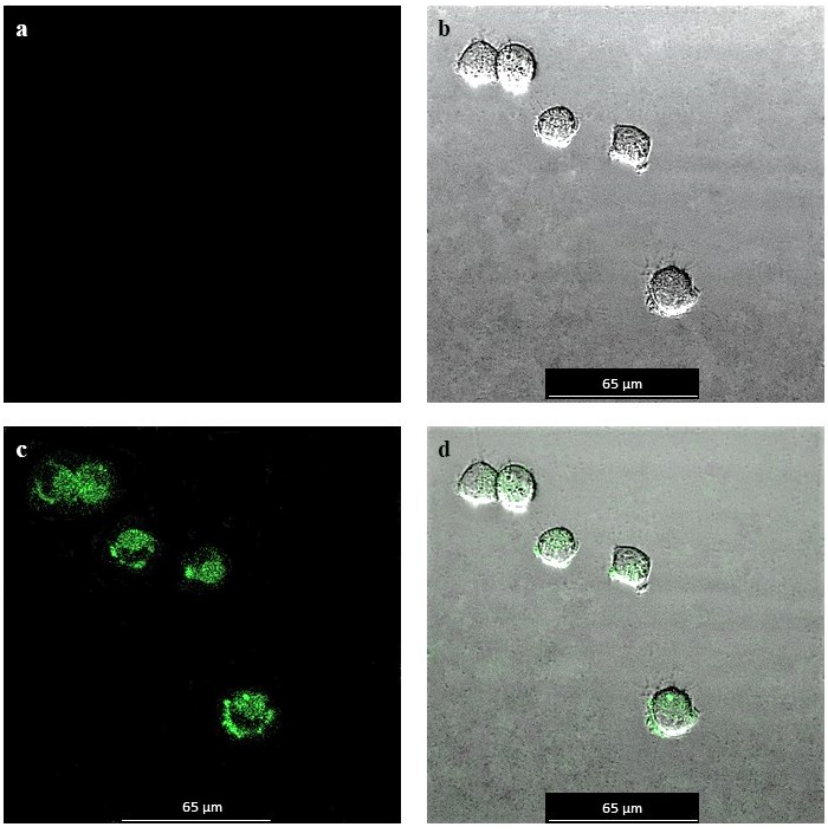

Figure 12. Confocal laser scanning for bright field and fluorescence imaging in Cath-a-differentiated cells (**a**) Cath-a-differentiated cells were incubated with **RdN** (10 µM) for 30 min at 37 °C. (**b**) The bright-field image of cells is shown in panel a. (**c**) Fluorescent images of cells with 10 µM **RdN** and further incubated with Pb^{2+} (10 µM) for 30 min at 37 °C. (**d**) an overlay image of (**b**, **c**).

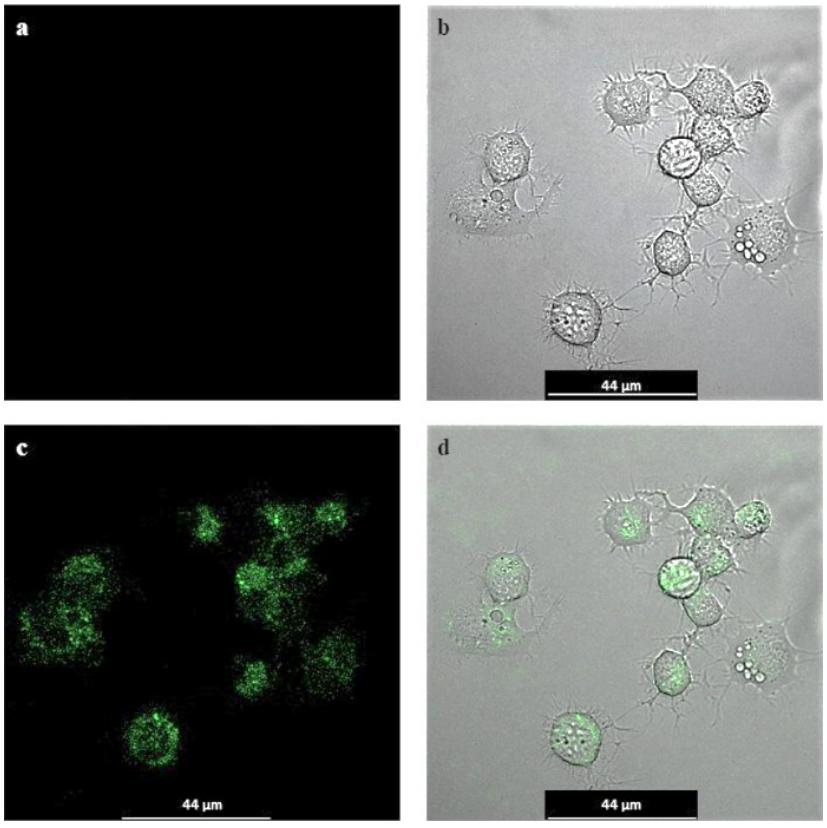

Figure 13. Confocal laser scanning for bright field and fluorescence imaging in Cath-a-differentiated cells (**a**) Cath-a-differentiated cells were incubated with **RdN** (10 μM) for 30 min at 37 °C. (**b**) The bright-field image of cells is shown in panel **a**. (**c**) Fluorescent images of cells with 10 μM **RdN** and incubated with Cu^{2+} (10 μM) for 30 min at 37 °C. (**d**) an overlay image of (**b**, **c**).

3. Experimental Section

3.1. Materials and Instrumentation

All solvents and reagents were received from Sigma-Aldrich (St. Louis, MO, USA), including 3-hydroxy-2-naphthoic hydrazide, rhodamine 6 G, glyoxal, methanol, and acetonitrile, and used without further purification. The salt solutions prepared nitrate [$Al(NO_3)_3$, $Cr(NO_3)_3$, $Zn(NO_3)_2$, $Ni(NO_3)_2$, $NaNO_3$, $Mg(NO_3)_2$, $Pb(NO_3)_2$, $Cd(NO_3)_2$, KNO_3] or chlorides [$CuCl_2$, $FeCl_3$, $CaCl_2$], and tetrabutylammonium anion salts. The stock solution salt cations (1×10^{-3} M), anions (1×10^{-4} M), and compound **RdN** (1×10^{-3} M**)** were prepared in CH_3CN/H_2O. The target compounds were synthesized in a CEM microwave reactor (CEM Corporation, Mathews, NC, USA). ^{1}H-NMR and ^{13}C-NMR spectra were recorded using a Bruker 400 MHz spectrometer (Billerica, MA, USA). DMSO-d_6 and TMS were used as solvents and internal standards for NMR spectra analysis. A Bruker 12 T Solaris FT-ICR-MS (Billerica, MA, USA) was used to record high-resolution mass spectrometry (HR-MS). The fluorescence and absorption spectra were recorded using a Cary Eclipse fluorescence spectrophotometer and an Agilent Cary 60 UV/Vis spectrometer (Greenwood Pl, Savage, MD, USA).

3.2. Cytotoxicity and Bioimaging in CAD Cells

Cath-a-differentiated (CAD) cells were used in cytotoxicity and bioimaging studies. Dulbecco's Modified Eagles Medium (DMEM), 10% fetal bovine serum (FBS), streptomycin medium, and 1% penicillin G were used for cell culture [11,12]. Cell cultures are maintained at 37 °C in a humidified atmosphere containing 5.0% CO_2 [11]. A Leica STELLARIS 5 confocal microscope (Deerfield, Illinois, USA) and BioTek Synergy H1 plate reader were used for fluorescence imaging and optical density studies of cytotoxicity [13].

3.3. Microwave-Assisted Synthesis of RdN

The rhodamine-based derivative is synthesized according to the literature [14]. A synthetic step for compound **RdN** is depicted in Scheme 1. Rhodamine Rd1 (100 mg, 0.219 mmol), 3-hydroxy-2-naphthoic hydrazide (46 mg, 0.219 mmol), and 2 mL methanol were mixed in a 10 mL reaction vial and placed in the cavity of a CEM microwave reactor. The reaction mixture was run under pressure and irradiated at 100 °C for 30 min. Then, the resulting solid was filtered and washed three times with cold ethanol. The product, the yellow powder, was isolated to give an 87% yield. ^{1}H-NMR (DMSO-d_6), δ (ppm): 11. 87 (1H, s), 10.95 (1H, s), 8.26 (1H, s, J = 7.5 Hz, N=C-H); 7.85 (4H, m), 7.72 (1H, J = 7.5 Hz, d), 7.53 (3H, m), 7.49 (1H, 7.5 Hz, t), 7.26 (1H, s, J = 7.5 Hz, H-Ar), 6.99 (1H, d, H-Ar), 6.36 (2H, s), 6.19 (2H, s), 5.14 (3H, m), 3.40 (4H, q, NCH_2CH_3), 1.86 (6H, s, -CH_3), 1.19 (6H, t, NCH_2CH_3). ^{13}C-NMR (DMSO-d6), δ (ppm): 192.76, 164.23, 153.21, 151.52, 148.77, 147.68, 134.30, 133.52, 130.44, 129.25, 127.90, 126.60, 124.23, 123.57, 108.31, 106.36, 97.99, 66.32, 44.08, 12.84. HRMS (MALDI): m/z Calculated for $C_{40}H_{37}N_5O_4$:653.2870; Found: 653.2887

3.4. Computational Studies

The molecule's ground-state geometries were optimized at the density functional theory (DFT) level using a hybrid B3LYP level of theory, a LanL2DZ basis set in the gas phase, water media, and simulated CH_3CN using a conductor-like polarizable continuum

model (CPCM). All computations were carried out using Spartan '20 and '24 software packages.

4. Conclusions

A colorimetric and fluorescent rhodamine-based sensor was developed to detect Pb^{2+} and Cu^{2+} ions in aqueous solution. Within the CH_3CN/H_2O (9:1, v/v) tris-HCl buffer solution, it was noticed that the sensor exhibited a greater degree of selectivity towards Pb^{2+} and Cu^{2+} regardless of other metal ions. The opening of the spirolactam ring, which occurs because of Pb^{2+} and Cu^{2+} ions, is the most crucial factor in sensing both ions. According to Job's plot analysis, the stoichiometry of Pb^{2+} and Cu^{2+} binding to sensor **RdN** was proposed to be 1:2. The detection limit of Pb^{2+} and Cu^{2+} ions was calculated to be 0.112 μM and 0.130 μM μM, respectively. According to cytotoxicity and confocal fluorescence imaging, the probe **RdN** can detect Pb^{2+} and Cu^{2+} in living cells. ~~Also~~Moreover, computational studies provided computational insights with respect to the properties of **RdN,** bis-(**RdN**)$_2Pb^{2+}$, and bis-(**RdN**)$_2Cu^{2+}$.

Author Contributions: Conceptualization, F.A.; Methodology, F.A., R.S., S.U., I.A. and J.W.; Investigation, O.A., R.S., S.U. and I.A.; Resources, F.A. and J.W.; Writing – original draft, F.A.; Supervision, F.A.; Project administration, F.A.; Funding acquisition, F.A. All authors have read and agreed to the published version of the manuscript.

Supplementary Materials: The following supporting information can be downloaded at https://www.mdpi.com/article, Figure S1; Fluorescence lifetime measurements of RdN and Pb^{2+} complex; Figure S2: HRMS spectra of compound R1 (MALDI positive mode); Figure S3: Proton NMR spectra of compound RdN (DMSO-d_6, 400MHz); Figure S4: ^{13}C- NMR spectra of compound RdN (DMSO-d_6, 400MHz); Figure S5: HRMS spectra of compound RdN (MALDI positive mode).

Funding: This research was supported by the National Science Foundation's Division of Chemistry under grant [2100629].

Acknowledgment

The authors acknowledge the Morgan State University's Molecular and Cellular Biology core lab for providing instruments

Data Availability: The data presented in this study are available on request from the corresponding author.

Acknowledgments: The authors acknowledge Morgan State University's core lab for providing the necessary facilities.

Conflicts of Interest: The authors declare no conflicts of interest.

References

1. Hijji, Y.; Rajan, R.; Shraim, A. 3-Aminopyridine salicylidene: A sensitive and selective chemosensor for the detection of Cu (II), Al(III), and Fe(III) with application to real samples. *Int. J. Mol. Sci.* **2022**, *23*, 13113.
2. Su, W.; Yuan, S.; Wang, E. A Rhodamine-based fluorescent chemosensor for the detection of Pb^{2+}, $Hg^{2+,}$ and Cd^{2+}. *J. Fluoresc.* **2017**, *27*, 1871–1875.
3. Xie, X.; Pan, M.; Hong, L.; Liu, K.; Yang, J.; Wang, S.; Wang, S. An "Off–On" Rhodamine 6G hydrazide-based output platform for fluorescence and visual dual-mode detection of lead (II). *J. Agric. Food Chem.* **2021**, *69*, 7209–7217.
4. Kwon, J.; Jang, Y.; Lee, Y.; Kim, K.; Seo, M.; Nam, W.; Yoon, J. A highly selective fluorescent chemosensor for Pb^{2+}. *J. Am. Chem. Soc.* **2005**, *127*, 10107–10111.
5. Gao, T.; Lee, K.; Yang, S. Synthesis and characterization of rhodamine based Pb^{2+} selective fluorescence sensor. *Toxicol. Environ. Health Sci.* **2009**, *1*, 159–162.
6. Wu, F.Y.; Zhang, H.; Xiao, M.; Han, B.X. A dual colorimetric and fluorescent sensor for lead ion based on naphthalene hydrazone derivative. *Spectrochim. Acta Part A Mol. Biomol. Spectrosc.* **2013**, *109*, 221–225.

7. Silpcharu, K.; Soonthonhut, S.; Sukwattanasinitt, M.; Rashatasakhon, P. Fluorescent sensor for copper and cyanide ions via the complexation-decomplexation mechanism with di(bissulfonamido)sprobifluorene. *ACS Omega* **2021**, *6*, 16696–16703.
8. Guo, T.; Tian, R.; Qu, W.; Yang, B.; Geng, Z.; Wang, Z. A near-infrared turn-on fluorescent sensor for the determination of copper in mitochondria. *Dye. Pigment.* **2022**, *205*, 110483.
9. Yu, H.; Lee, Y.J.; Angupillai, S.; Wang, S.; Feng, S.; Matsumoto, S.; Son, Y.A. A new dual fluorogenic and chromogenic "turn-on" chemosensor for Cu^{2+}/F^- ions. *Spectrochim. Acta Part A Mol. Biomol. Spectrosc.* **2015**, *151*, 48–55.
10. Mohanasundaram, D.; Bhaskar, R.; Sankarganesh, M.; Nehru, K.; Kumar, G.; Rajesh, J. A simple pyridine based fluorescent chemosensor for selective detection of copper ion. *Spectrochim. Acta Part A Mol. Biomol. Spectrosc.* **2022**, *265*, 120395.
11. Qi, Y.; Wang, J.; McMillian, M.; Chikaraishi, D.M. Characterization of a CNS cell line, CAD, in which morphological differentiation is initiated by serum deprivation. *J. Neurosci.* **1997**, *17*, 1217.
12. Nyan, D.C.; Anbazhagan, R.; Hughes-Darden, C.A.; Wachira, J. Endosomal Colocalization of Melanocortin-3 Receptor and Beta-Arrestins in CAD Cells with Altered Modification of AKT/PKB. *Neuropeptides* **2008**, *42*, 355–366.
13. He, H.; Cheng, Z.; Zheng, L.; Zhang, X. Evaluation of Fluorescent Pb^{2+} Probes: Instant Sensing, Cell Permeable Recognition and Quantitative Detection. *Molecules* **2021**, *26*, 512.
14. Aduroja, O.; Abiye, I.; Fathima, A.; Tadesse, S.; Ozturk, B.; Wachira, J.; Abebe, F. Microwave-assisted synthesis for a highly selective rhodamine 6G-derived fluorescent sensor and bioimaging. *Inorg. Chem. Commun.* **2023**, *147*, 110236.
15. Aduroja, O.; Shaw, R.; Abebe, F. A bis(rhodamine 6G)-based fluorescent sensor for Hg^{2+}: Microwave-assisted synthesis, photophysical properties, and computational studies. *Res. Chem. Intermed.* **2022**, *48*, 1847–1861.
16. Li, L.Q.; Meng, L.P. Novel rhodamine derivative as high selective detection lead sensor. *Spectrochim. Acta A Mol. Biomol. Spectrosc* **2014**, *122*, 772–775.
17. Liu, T.; Wan, X.; Yao, Y. Dual sensitive and selective sensor for Pb^{2+} and Al^{3+} with distinctive fluorescence response *Sens. Actuators B* **2018**, *254*, 1094–1100.
18. Wan, J.; Zhang, K.; Li, C.; Niu, S. A novel fluorescent chemosensor based on a rhodamine 6G derivative for the detection of Pb^{2+} ion. *Sens. Actuators B* **2017**, *246*, 696–702.
19. Abebe, F.; Sutton, T.; Perkins, P.; Shaw, R. Two colorimetric fluorescent turn-on chemosensors for detection of Al^{3+} and N_3^-: Synthesis, photophysical, and computational studies. Luminescence **2018**, 33(7), 1194-1207.
20. Iniya, M.; Vidya, B.; Anand, T.; Sivaraman, G.; Jeyanthi, D.; Krishnaveni, K.; Chellappa, D. Microwave-assisted synthesis of imidazquinazoline for chemosensing of Pb^{2+} and Fe^{3+} and living cell application. *ChemistrySelect* **2018**, *3*, 1282–1288.
21. Meng, X.; Cao, D.; Hu, Z.; Han, X.; Li, Z.; Ma, W. A highly sensitive and selective chemosensor for Pb^{2+} based on quinolone-coumarin. *RSC Adv.* **2018**, *8*, 33947–33951.
22. Prabhu, J.; Velmurugan, K.; Nandhakumar, R. Development of fluorescent lead II sensor based on an anthracene derived chalcone. *Spectrochim. Acta A Mol. Biomol. Spectrosc.* **2015**, *144*, 23–28.
23. Li, C.Y.; Zhou, Y.; Li, Y.F.; Kong, X.F.; Xou, C.X.; Weng, C. Colorimetric and fluorescent chemosensor for citrate based on a rhodamine and Pb^{2+} complex in aqueous solution. *Anal. Chim. Acta* **2013**, *774*, 79–84.
24. Karak, D.; Banerjee, A.; Lohar, S.; Sahana, A.; Mukhopadhyay, S.; Adhikari, S.; Das, D. Xanthone based Pb^{2+} selective turn-on fluorescent probe for living cell staining. *Anal. Methods* **2013**, *169*, 169–172.
25. Zhu, J.; Yeo, J.; Bowyer, A.; Proschogo, N.; New, E.J. Studies of the labile lead pool using a rhodamine-based fluorescent probe. *Metallomics* **2020**, *12*, 644–648.
26. Fu, Z.H.; Yan, L.B.; Zhang, X.; Zhu, F.F.; Han, X.L.; Fang, J.; Wang, Y.W.; Peng, Y. A fluorescein-based chemosensor for relay fluorescence recognition of Cu(II) ions and biothiols in water and its applications to a molecular logic gate and living cell imaging. ***Org. Biomol. Chem.*** **2017**, ***15***, 4115–4121.
27. Zavalishin, M.; Gamov, G.; Kiselev, A.; Nikitin, G. A fluorescein conjugates as colorimetric and red-emissive fluorescence chemosensor for selective recognition Cu^{2+} ions. *Opt. Mater.* **2024**, *153*, 115580.
28. Mahajan, P.; Dige, N.; Vanjare, B.; Eo, S.; Kim, S.; Lee, K. A nano sensor for sensitive and selective detection of Cu^{2+} based on fluorescein: Cell imaging and drinking water analysis. *Spectrochim. Acta A Mol. Biomol. Spectrosc.* **2019**, *216*, 105–116.
29. Wang, Y.; Chang, H.Q.; Wu, W.N.; Peng, W.B.; Yan, Y.F.; He, C.M.; Chen, T.; Zhao, X.L.; Xu, Z. Rhodamine 6G hydrazone bearing pyrrole unit: Ratiometric and selective fluorescent sensor for Cu^{2+} based on two different approaches. *Sens. Actuators* **2016**, *228*, 395–400.
30. Abebe, F.; Perkins, P.; Shaw, R.; Tadesse, S. A rhodamine-based fluorescent sensor for selective detection of Cu^{2+} in aqueous media: Synthesis and spectroscopic properties. *J. Mol. Struct.* **2020**, *1205*, 127594.

31. Cho, H.; Chae, J.B.; Kim, C. A thiophene-based blue-fluorescent emitting chemosensor for detecting indium (III) ion. *Inorg. Chem. Commun.* **2018**, *97*, 171–175.